Earth and Planetary Science Letters 499 (2018) 74–82

Contents lists available at ScienceDirect

Earth and Planetary Science Letters

www.elsevier.com/locate/epsl

Dynamics of rheological heterogeneities in mantle plumes

Cinzia G. Farnetani [a,*], Albrecht W. Hofmann [b,c], Thomas Duvernay [a,1], Angela Limare [a]

[a] Institut de Physique du Globe de Paris, Sorbonne Paris Cité, Université Paris Diderot, UMR 7154, 75005 Paris, France
[b] Lamont-Doherty Earth Observatory of Columbia University, Palisades, NY 10964, USA
[c] Max-Planck-Institut für Chemie, Hahn-Meitner-Weg 1, 55128 Mainz, Germany

ARTICLE INFO

Article history:
Received 23 March 2018
Received in revised form 9 July 2018
Accepted 17 July 2018
Available online 30 July 2018
Editor: J. Brodholt

Keywords:
rheology
mixing
mantle plume
dynamics
heterogeneity

ABSTRACT

The geochemical record of Hawaiian basalts has been interpreted to reflect vertically stretched, partly filament-like heterogeneities in the Hawaiian plume, but one alternative interpretation has been that this record reflects intra-conduit mixing, caused by rheological contrasts across the conduit. Here we present numerical simulations of a mantle plume carrying rheological heterogeneities λ times more viscous than the surrounding fluid. Our first objective is to quantify how the heterogeneity deforms during upwelling. We find a full spectrum of shapes, from stretched filaments to nearly undeformed blobs, and we map the respective stability domain as a function of the viscosity ratio λ and of the flow characteristics, including the plume buoyancy flux. Our second objective is to test the hypothesis that a rheological heterogeneity can cause intra-conduit mixing. Although horizontal velocities do appear across the plume conduit, we have not found any toroidal "doughnut-shaped swirl" mode. Instead we show that perturbations of the flow trajectories are a local phenomenon, unable to cause permanent mixing. Our third objective is to determine over which time-scales a rheological heterogeneity crosses the magma capture zone (MCZ) beneath a hotspot volcano. For a blob-like heterogeneity of radius 30–40 km and viscosity ratio 15–20, the crossing time-scale is less than 1 Myr. Contrary to a stretched filament, a blob can entirely fill the MCZ, thereby representing the unique source rock of partial melts feeding a volcano. If the heterogeneity has a distinct isotopic fingerprint (or a distinct fertility), surface lavas will then record an isotopic fluctuation (or a fluctuation in melt productivity) lasting 0.5–0.8 Myr. Our simulations predict that such fluctuations should occur preferentially in low buoyancy flux hotspots, where blob-like rheological heterogeneities are more easily preserved than in the vigorous Hawaiian plume.

1. Introduction

Most geodynamic studies, from Becker et al. (1999) to Ballmer et al. (2017), share the idea that rheological heterogeneities in the Earth's mantle have large dimensions, with a radius ranging from several hundred to a thousand kilometers. A key issue is then to determine under which conditions the heterogeneous volumes can "survive" in the large scale mantle flow and whether they might represent long-lasting geochemical reservoirs. Here we change perspective and focus on small scale (30–50 km radius) rheological heterogeneities deformed by the three-dimensional flow of a thermal plume. A heterogeneity initially embedded in the basal thermal boundary layer, source region of plumes, has a complex deformation history which includes pure shear, while converging to the plume stem, and simple shear once in the conduit (Farnetani and Hofmann, 2009). It is also noteworthy that strain rates vary non-linearly across the plume conduit and their values are up to two orders of magnitude higher than in the convecting mantle (Cordier et al., 2012). Previous studies on the deformations of rheological heterogeneities did not consider these specific aspects of the plume flow, either because they analyzed pure shear and simple shear separately (Cox, 1969; Spence et al., 1988; du Merveilleux and Fleitout, 2001) or because they used two-dimensional kinematically-driven models (Manga, 1996). Clearly, results obtained with large-scale circulation models cannot be extrapolated to the plume flow, as illustrated by the case of a heterogeneity with viscosity ratio $\lambda = \eta_h/\eta = 1$, where η_h is the viscosity of the heterogeneity and η the viscosity of the surrounding fluid. In a large-scale circulation model a $\lambda = 1$ heterogeneity is moderately deformed, even after a complete mantle overturn (Manga, 1996), whereas a passive heterogeneity rising into a plume

* Corresponding author.
E-mail addresses: cinzia@ipgp.fr (C.G. Farnetani), albrecht.hofmann@mpic.de (A.W. Hofmann), thomas.duvernay@anu.edu.au (T. Duvernay), limare@ipgp.fr (A. Limare).
[1] Now at Research School of Earth Sciences, The Australian National University, Canberra, ACT, 2601, Australia.

https://doi.org/10.1016/j.epsl.2018.07.022
0012-821X/

is stretched into a filament (Farnetani and Hofmann, 2009). It is thus relevant to ask if such a contrasting behavior persists for heterogeneities which are intrinsically more viscous ($\lambda > 1$) than the surrounding fluid.

Pioneering laboratory experiments by Taylor (1934) showed that pure shear leads to exponential stretching, independently of the viscosity ratio, whereas for simple shear Manga (1996) defined a "threshold value": if $\lambda < 4$ the heterogeneity is linearly stretched, if $\lambda > 4$ the heterogeneity rotates with minor deformation. In order to test whether this "threshold value" applies to the plume flow, we conducted numerical simulations where we calculate the deformation of rheological heterogeneities for a wide range of viscosity ratios and flow characteristics.

Besides the deformation of the heterogeneity, we study to which extent a rheological heterogeneity perturbs the flow of the surrounding fluid, because lateral viscosity variations can induce a toroidal flow component within a poloidal flow (O'Connell et al., 1991; Bercovici et al., 2000). Just as a reminder, the toroidal flow is associated with rotations in a horizontal plane, whereas the poloidal, buoyancy driven, flow is associated with upwellings and downwellings. Using mantle circulation models driven by surface motion, Ferrachat and Ricard (1998) concluded that mantle mixing is enhanced when both poloidal and toroidal components are present. Although the plume flow is clearly poloidal, rheological contrasts across the conduit could favor the appearance of a toroidal flow component which would cause intra-conduit mixing, as argued by Blichert-Toft and Albarède (2009). A quantitative understanding of intra-conduit mixing is fundamental to interpret the spatio-temporal isotopic variability observed in hotspot lavas. For example, the bilateral zonation of Hawaiian volcanoes, forming the Kea- and Loa-trends, has been interpreted to reflect isotopically distinct areas in the deep-mantle (Abouchami et al., 2005; Weis et al., 2011; Huang et al., 2011). The idea that the isotopic zonation in the plume conduit preserves a "memory" of the large-scale zonation in the source region implies insignificant intra-conduit mixing. This requirement is satisfied for thermal plumes advecting passive heterogeneities (Farnetani et al., 2012), but is not satisfied for thermo-chemical plumes, since compositionally denser material rises preferentially at the plume axis (Jones et al., 2016).

A complex aspect of intrinsic viscosity contrasts (i.e., those not due to temperature differences) is that the rheology of mantle rocks depends on several parameters. Plastic deformation of rocks occurs either by dislocation creep (i.e., motion of dislocations) or by diffusion creep (i.e., diffusive transport of atoms). For diffusion creep, which dominates in most of the lower mantle, viscosity is directly related to the diffusion coefficients. Because silicon is one of the slowest diffusing species (Yamazaki et al., 2000), a Si increase likely leads to a viscosity increase, as supported by early studies on the activation energies (Weertman, 1970) and on melting temperatures of perovskite and periclase (Zerr and Boehler, 1994). Viscosity also increases with the square of the mineral grain size (Ammann et al., 2010) and it varies with water content (Katayama and Karato, 2008; Karato, 2010), thus rocks that experienced an efficient fluid removal should be more viscous than the surrounding peridotites (Hirth and Kohlstedt, 1996). Last but not least, for a mineral assemblage of a weak and a strong component, the bulk viscosity depends on the volume fraction and on the geometry of the weak component (Takeda, 1998). More specifically, when the weak MgO periclase (Cordier et al., 2012) forms isolated grains the bulk viscosity is 10–1000 times higher than when MgO periclase forms a continuous film (Yamazaki and Karato, 2001). In our work, we model rheological heterogeneities without specifying their mineral assemblage, bulk composition, grain size and fluid content; only in the Discussion we hypothesize that rheological heterogeneities might carry a distinct isotopic signature or have a distinct fertility to melt production. This hypothesis will enable us to predict time-scale of isotopic variability, or of fluctuation in melt productivity, caused by a rheological heterogeneity crossing the melting zone beneath a hotspot volcano.

2. Model setup

The geodynamic code Stag3D (Tackley, 1998) solves the equations governing conservation of mass, momentum and energy for an incompressible viscous fluid at infinite Prandtl number. The size of the cartesian domain in the $X{:}Y{:}Z$ directions is 2200:2200:2900 km, and the grid size ranges from 8 to 10 km/cell. The physical parameters used to calculate the Rayleigh number

$$Ra = \frac{\rho g \alpha \Delta T d^3}{\eta_m \kappa} \tag{1}$$

are the mantle density $\rho = 4000$ kg m^{-3}, the thermal expansion coefficient $\alpha = 3 \times 10^{-5}$ K^{-1}, the maximum potential temperature contrast $\Delta T = 1950$ K, the depth $d = 2900$ km, the mantle viscosity $\eta_m = 10^{22}$ Pa s and the thermal diffusivity $\kappa = 10^{-6}$ m^2 s^{-1}. Similar to van Keken et al. (2013), a thermal plume is generated at the bottom of the model domain over a heated patch of radius $r_p = 500$ km and maximum excess potential temperature $\delta T_p = 600\,^\circ$C. Viscosity is temperature dependent:

$$\eta(T) = \eta_m \exp\left[\frac{E}{R}\left(\frac{T_m - T}{T_m T}\right)\right], \tag{2}$$

where $T_m = 1350\,^\circ$C the mantle potential temperature, R the gas constant, E the activation energy. For the reference model $E = 220$ kJ mol^{-1}, but we vary the activation energy over a range going from 140 kJ mol^{-1} to 300 kJ mol^{-1}. A rheological heterogeneity λ times more viscous than the surrounding fluid is simulated using 7×10^6 tracers. The heterogeneity is at an initial distance of 100 km form the plume axis, this distance is kept constant because it guarantees minimum temperature gradients across the heterogeneity, thereby avoiding to have a temperature-dependent viscosity variation superimposed on the intrinsic viscosity increase λ. At each time step the code calculates the number of tracers present in each grid cell, modifies the cell viscosity and calculates the resulting velocity field, which is then used to advect the tracers. As discussed by du Merveilleux and Fleitout (2001), a numerical method based on grid cells cannot accurately resolve a sharp viscosity interface. In view of this limitation, we conducted a series of tests to verify that the grid resolution is sufficiently accurate to resolve heterogeneities with an initial radius $R_i \geq 30$ km.

3. Results

Fig. 1 shows the evolving shape of an initial sphere ($R_i = 40$ km) as it rises in the plume conduit. The passive heterogeneity ($\lambda = 1$) is stretched into a filament (Fig. 1a), in agreement with Farnetani and Hofmann (2009). For viscosity ratio $\lambda = 10$ (Fig. 1b) we find a transitional shape resembling a "tadpole" with a blob-shaped lower part and an elongated, progressively stretched upper "tail". Finally, for viscosity ratio $\lambda = 20$ (Fig. 1c) the heterogeneity maintains a blob-like shape. In the following we focus on the flow field within and around the viscous heterogeneity, in order to understand the dynamic interaction between the heterogeneity and the surrounding flow. For the reference case without viscous heterogeneity the radial dependence of the vertical velocity (Fig. 2a, green dashed line) fits Olson et al. (1993) exponential law $v_z(r) = v_z^{axis} \exp(-Cr^2)$, where the value of the constant C depends on the activation energy and on the plume's temperature contrast. (Note that the radial distance from the plume axis

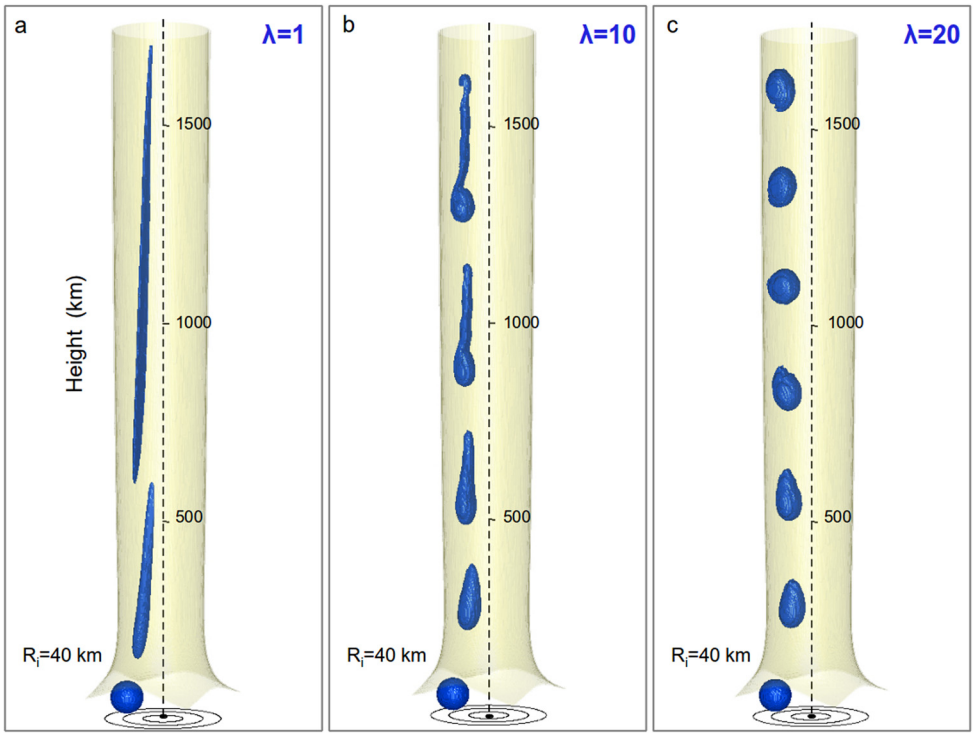

Fig. 1. Plume conduit with isosurface at excess potential temperature $\Delta T = 100\,^{\circ}\mathrm{C}$ (yellow shade). A single heterogeneity (blue) is at an initial distance of 100 km from the plume axis and has an initial spherical shape of radius $R_i = 40$ km. (a) For viscosity ratio $\lambda = 1$ the heterogeneity is shown at elapsed time 0, 12, 38 Myr. (b) For $\lambda = 10$, at elapsed time 0, 13, 25, 41, 51 Myr. (c) For $\lambda = 20$, at elapsed time 0, 13, 25, 38, 51, 63 and 76 Myr. (For interpretation of the colors in the figure(s), the reader is referred to the web version of this article.)

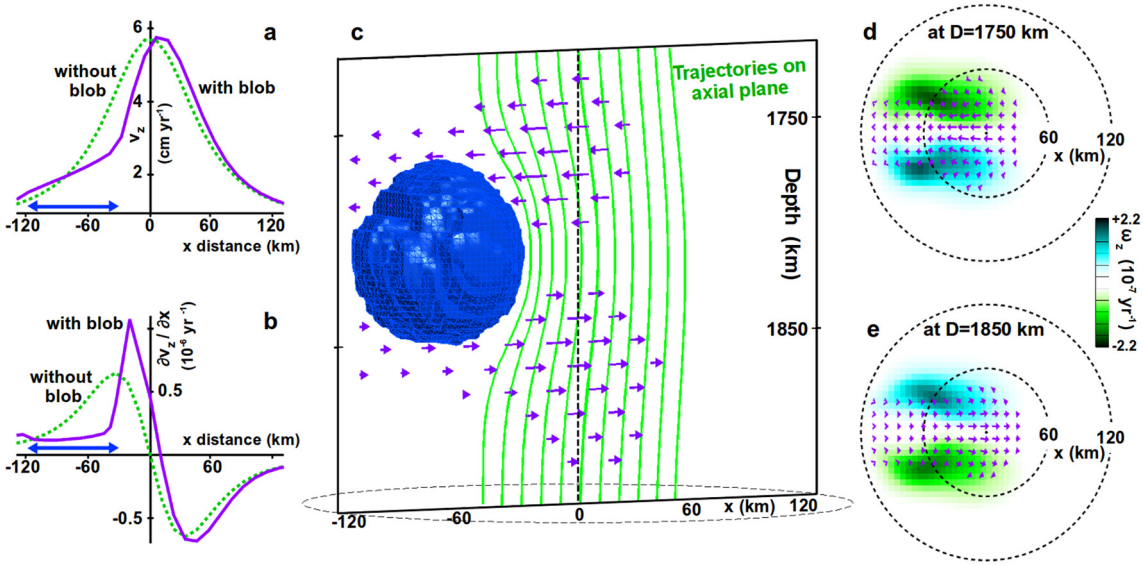

Fig. 2. (a) Vertical velocity profile for the case without blob (green dashed line) and with blob (violet line). The horizontal axis gives the x-distance from the plume axis; the blue arrow indicates the lateral extent of the blob. (b) The corresponding profile for $\partial v_z/\partial x$, the most important term of the shear $\dot{\epsilon}_{xz}$, without blob (green dashed line) and with blob (violet line). (c) Three-dimensional view of the viscous blob, $\lambda = 20$, $R_i = 40$ km, the blob center is at 1800 km depth. For graphical reasons the fluid flow trajectories (green lines) and the v_x velocity component (violet arrows) are shown only for one vertical plane. The distance between the plume axis (black dashed line) and the axial trajectory is at maximum of 11 km. The dashed circle indicates the 120 km radial distance from the plume axis. (d) Horizontal cross section at depth 1750 km (i.e., 50 km above the blob center), showing the horizontal velocity components (violet arrows), and the vorticity component ω_z (color shades). The dashed circles indicate the radial distance (120 km, 60 km) from the plume axis. (e) Same as above, but at depth 1850 km (i.e., 50 km below the blob center).

can be easily calculated using x and y coordinates in our cartesian geometry). In the presence of a rheological heterogeneity, the vertical velocity is reduced both inside the blob and in part of the conduit (Fig. 2a, violet line), so that the axial symmetry of the velocity profile is lost and the maximum v_z is displaced off-axis. Spatial variations of the vertical velocity have two important consequences: The first one is to modify the shear component

$$\dot{\epsilon}_{xz} = \frac{1}{2}\left(\frac{\partial v_x}{\partial z} + \frac{\partial v_z}{\partial x}\right), \tag{3}$$

in particular, the v_z reduction inside the blob induces a significant decrease of dv_z/dx (Fig. 2b), thereby reducing the shear $\dot{\epsilon}_{xz}$ and favoring the preservation of the blob-like shape. In the surrounding fluid instead dv_z/dx increases, creating a zone of high shear between the plume axis and the edge of the rheological het-

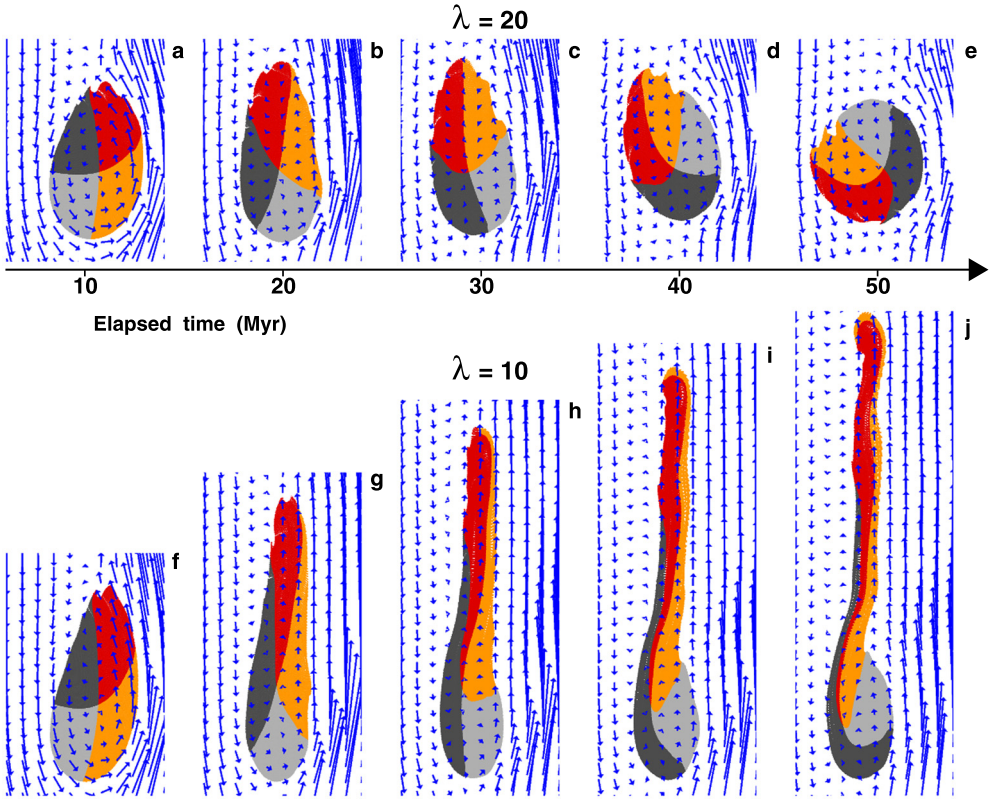

Fig. 3. The evolving shape of the heterogeneities for $R_i = 40$ km, $\lambda = 20$ (top panels) and $\lambda = 10$ (bottom panels). Colors keep track of the initial position of tracer particles and enable to visualize the internal rotation during ascent. Blue arrows indicate the residual velocity field (see text), so that at the blob center $\bar{v}_x = \bar{v}_z = 0$. The blob center is graphically visible where the four colors meet, and its coordinates [axial distance (km), height (km)] are: [48, 201] (a); [61, 413] (b); [66, 614] (c); [66, 817] (d); [65, 1090] (e); and [48, 203] (f); [62, 417] (g); [71, 618] (h); [77, 817] (i); [81, 1012] (j).

erogeneity. The second consequence is that, in an incompressible fluid, vertical velocity variations cause the appearance of horizontal velocity components, which are otherwise negligible across the conduit. Fig. 2c shows, besides the three-dimensional blob ($R_i = 40$ km, $\lambda = 20$), the horizontal velocities v_x and the flow trajectories (green lines) on the axial plane. The distribution of v_x can be understood by considering that the rheological heterogeneity, because of its reduced vertical velocity, represents an "obstacle" for the fluid column beneath the blob. This fluid tends to contour the blob, as illustrated by the flow trajectories, whose axial displacement is at maximum 11 km. The horizontal cross sections just above (Fig. 2d) and below (Fig. 2e) the blob indicate that a large part of the plume conduit is affected by the horizontal flow (violet arrows), where v_x can be as high as $0.3 v_z$. The tendency of the fluid element to spin is given by the vorticity vector $\omega = \nabla \times v$. For a horizontal section

$$\omega_z = \left(\frac{\partial v_y}{\partial x} - \frac{\partial v_x}{\partial y} \right) \tag{4}$$

corresponds to the toroidal flow component. We find that there is no net spin around the vertical axis because on each horizontal section (Fig. 2d–2e) ω_z has both a positive and a negative sign; $\omega_z \neq 0$ simply indicates that the horizontal flow has an azimuthal component. The selected horizontal sections are at a vertical distance of only 50 km above/below the blob center, however, at greater distance (e.g., 100 km) both v_x and the axial deviation of the trajectories become negligible (Fig. 2c). We conclude that the flow perturbation occurs in the "proximity" of the viscous heterogeneity (i.e., over a vertical extent $\sim 5 R_i$, for R_i of 30–40 km), and its local character does not generate permanent intra-conduit mixing.

Simple shear combines equal parts of vorticity, which leads to solid-body rotation, and of shear strain rate, which leads to stretching (Turcotte and Schubert, 1982). As first noticed by Taylor (1934), a viscous blob ($\lambda = 20$) in a simple shear flow will rotate more rapidly than it is stretched. To better understand the internal rotation we calculate the residual velocity vector ($\bar{v}$) by subtracting the velocity at the blob center (v^c). On a X–Z plane the two components are: $\bar{v}_x = v_x - v_x^c$ and $\bar{v}_z = v_z - v_z^c$. For the case $\lambda = 20$ (Fig. 3, top panels) the residual velocity field inside the blob is reminiscent of a solid body rotation (i.e., $\bar{v}_x = -Cz$, $\bar{v}_z = Cx$, where C is a constant and the blob center is at $x = 0$, $z = 0$). The appearance of the horizontal component is thus essential to reduce the deformation and to promote rotation. For the case $\lambda = 10$ (Fig. 3, bottom panels) the heterogeneity gradually develops a transitional, tadpole shape. The lower part, which rotates internally, maintains a blob-like shape, whereas the upper part becomes progressively elongated under the effect of the shear $\dot{\epsilon}_{xz}$ and of the traction $\dot{\epsilon}_{zz}$, the latter arises because inside the heterogeneity $dv_z/dz \neq 0$.

Our next objective is to quantify the deformation undergone by a rheological heterogeneity. In two-dimensions the deformation of an ellipse of length L and breadth B is given by $D = (L - B)/(L + B)$, but unfortunately D cannot be used for a three dimensional body with an irregular shape. As a proxy for deformation we calculate the surface ratio $\sigma = S_h/S_i$, where S_h is the surface area of the heterogeneity, calculated at a given mantle depth, and S_i is the surface area of the initial sphere. Fig. 4 shows σ *vs.* λ for different initial sizes of the heterogeneity (besides $R_i = 40$ km we consider 30 km and 50 km). At low viscosity ratio (i.e., $1 \leq \lambda < 5$), and quite independently of the initial size, the deformations are high ($\sigma \geq 3$), typical of "filament-like" shape. For intermediate viscosity ratios we find a "transitional" shape ($1.5 < \sigma < 3$) and we remark that, at a given λ, a small-size heterogeneity is less deformed than

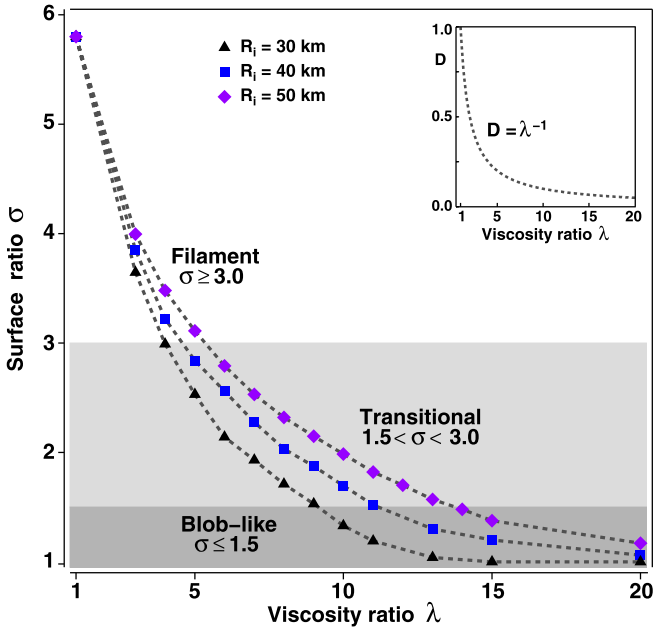

Fig. 4. Surface ratio $\sigma = S_h/S_i$ *vs.* viscosity ratio λ for three values of initial radius R_i. σ is calculated when the heterogeneity has risen 1500 km in the plume conduit, S_h is the surface area of the heterogeneity, S_i the surface area of the initial sphere. Values of σ enable to classify the shape of the heterogeneity in three categories: filament ($\sigma \geq 3$), transitional ($1.5 < \sigma < 3$), blob-like ($\sigma \leq 1.5$). In the inset: the trend $D = \lambda^{-1}$ (see text), where the length ratio D defines deformations of a two-dimensional ellipsoid.

a larger one. For $\lambda = 20$, values of σ are close to 1 and we define as "blob-like" all shapes with $\sigma \leq 1.5$. The inset of Fig. 4 shows the $D = \lambda^{-1}$ trend predicted by Taylor (1934) for a two-dimensional case with negligible interfacial tension. Our deformations, albeit calculated in a different way, decrease less rapidly than the λ^{-1} trend, and this occurs for two reasons: First, for a heterogeneity flowing in a mantle plume, the deformation history is not limited to simple shear, but also includes an earlier phase of pure shear when the heterogeneity converges towards the base of the conduit. Second, the trend $D = \lambda^{-1}$ assumes that the size of the heterogeneity is small with respect to the length-scale of the flow causing the deformation. Clearly, this cannot be assumed in our case since the size of the heterogeneity (i.e., its diameter, which is of order 60–100 km, depending on R_i) is not small with respect to the length-scale of the flow causing the deformation (i.e., the conduit radius 120–150 km). By relaxing the key assumption that the size of the heterogeneity is small with respect to the length-scale of the flow causing the deformation, and by considering the fully three-dimensional flow, we find that previous results cannot be extrapolated to the plume case.

We now consider the fate of viscous heterogeneities once in the plume head. Fig. 5a shows the melting zone, calculated using the dry solidus of Katz et al. (2003), and viscous heterogeneities ($R_i = 30$ km) with $\lambda = 1$ the filament, $\lambda = 5$ the transitional-shape, and $\lambda = 15$ the blob, shown at two time-steps. Given the different shapes and lengths of the heterogeneities, the time required to cross the melting zone is expected to vary significantly. Rather than considering the whole melting zone we focus on the volume of an ideal magma capture zone (MCZ). Following DePaolo and Stolper (1996) the MCZ beneath a volcano is schematized as a cylinder of radius $R_{MCZ} = 25$ km and of height equal to the melting column (i.e., $h_{MCZ} \sim 50$ km). As the heterogeneity flows through the MCZ at an upwelling velocity of 10–15 cm yr^{-1}, we calculate the volume of the heterogeneity inside the MCZ and we normalize it over the MCZ volume. This volume ratio is plotted in Fig. 5b *vs.* the transit time of the heterogeneity across the MCZ.

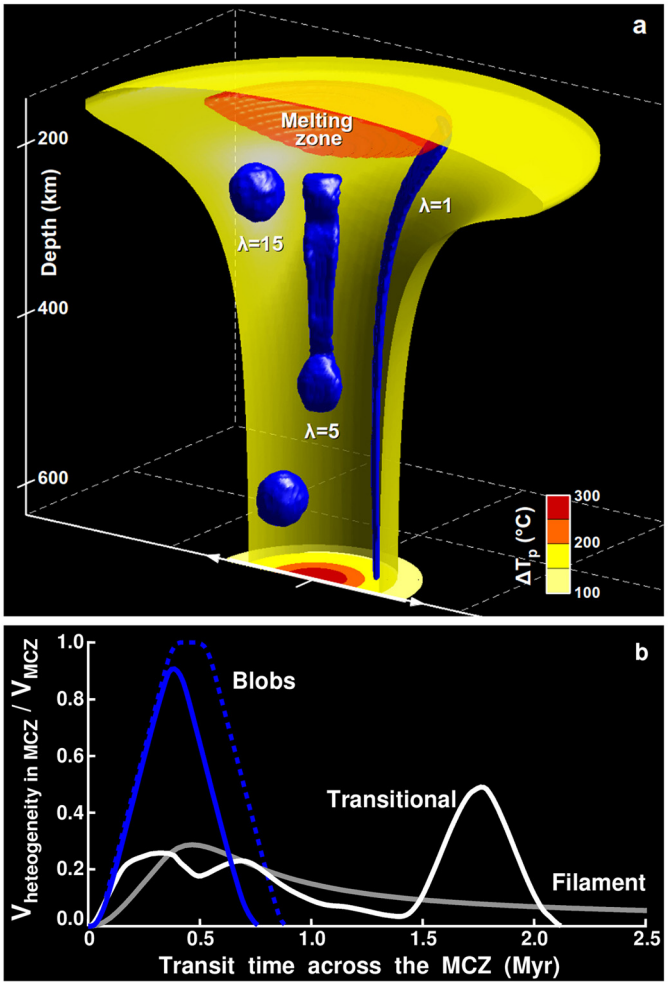

Fig. 5. (a) Plume head (yellow isosurface at excess potential temperature $\Delta T_p = 150\,^{\circ}$C) with the melting zone (orange shades) and the plume conduit (colors across the horizontal section correspond to ΔT_p, see color scale). For graphical reasons several heterogeneities (blue) are represented together, all have initial radius $R_i = 30$ km, but different viscosity ratio: $\lambda = 1$ for the filament, $\lambda = 5$ for the transitional shape, $\lambda = 15$ for the blob, shown at two time steps. (b) Transit time of the heterogeneity across the magma capture zone (MCZ) *vs.* the volume ratio $V_{heterogeneity\ in\ MCZ}/V_{MCZ}$. Solid lines are for the heterogeneities shown above ($R_i = 30$ km): the blob (blue line), the transitional shape (grey line), the filament (white line), whose transit time lasts more than 4 Myr (not shown in the figure). The blue dashed line for a blob with $R_i = 40$ km and $\lambda = 20$.

The blob, because of its compact shape, can fill the entire MCZ and its transit time is relatively short (0.5–0.8 Myr). In contrast, the long and narrow filament fills ~10–20% of the MCZ volume, and the transit time is longer than 4 Myr (not shown in the figure). The transitional, tadpole shape shows a precursory phase (volume fraction in the MCZ ~20%) lasting 1.0–1.5 Myr before the main arrival, where the volume fraction in the MCZ is ~50%. The implications of these results will be presented in the Discussion.

3.1. Effect of varying the plume flow

In the previous paragraph we varied λ and R_i of the heterogeneity, while keeping unchanged the physical parameters governing the plume flow. Here we explore the effect of varying the plume flow and this is accomplished by systematically varying the activation energy E, the plume buoyancy flux B, and by including a viscosity jump at 660 km depth.

The activation energy governs the temperature dependence of mantle viscosity and, rather than assuming $E = 220$ kJ mol^{-1}, we now span a range of plausible values ($140 \leq E \leq 300$ kJ mol^{-1}).

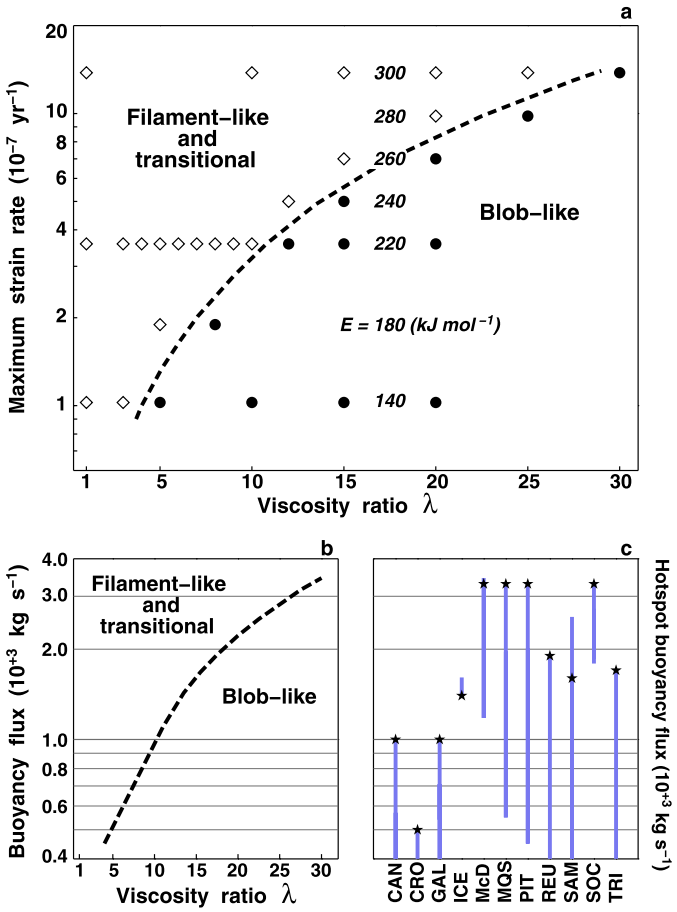

Fig. 6. (a) Stability field of blob-like and filament-transitional shapes ($R_i = 40$ km) as a function of λ and of the maximum strain rate component $\dot{\epsilon}_{xz}$ across the plume conduit. A range of $\dot{\epsilon}_{xz}$ values has been obtained by systematically varying the activation energy ($140 \leq E \leq 300$ kJ mol^{-1}) around the reference value $E = 220$ kJ mol^{-1}. The dashed line has the purpose of separating two domains corresponding to the filament-like and blob-like stability fields. (b) Stability field of blob-like and filament-transitional shapes ($R_i = 40$ km) as a function of the plume buoyancy flux. (c) Hotspot buoyancy flux from Sleep (1990) (black star) and the range (blue bar) by King and Adam (2014). The hotspots are: Canary (CAN), Crozet (CRO), Galápagos (GAL), Iceland (ICE), McDonald (McD), Marquesas (MQS), Pitcarn (PIT), Réunion (REU), Samoa (SAM), Society (SOC), Tristan (TRI).

The effect of increasing E is to increase both v_z and the maximum strain rate $\dot{\epsilon}_{xz}$ across the conduit. Fig. 6a shows that as $\dot{\epsilon}_{xz}$ increases the stability domain of the blob-like shape is progressively restricted to higher λ. More specifically, for $R_i = 40$ km, we find that at $\dot{\epsilon}_{xz} \sim 10^{-6}$ yr^{-1} ($E = 280$ kJ mol^{-1}) the blob-like shape is stable only if $\lambda > 20$, whereas if $\dot{\epsilon}_{xz}$ is one order of magnitude lower ($E = 140$ kJ mol^{-1}) the blob-like shape is stable at $\lambda = 4$, the value found by kinematically driven mantle circulation models (Manga, 1996).

For a constant activation energy ($E = 220$ kJ mol^{-1}) we varied the parameters used to generate the plume such as the excess temperature of the heated patch and its radius. This enabled us to obtain plumes with different buoyancy flux $B = \int v_z \rho \alpha \Delta T_p dS$, where the integral is over the conduit surface dS and ΔT_p is the plume excess temperature (Sleep, 1990). In the uppermost part of the lower mantle our models have a plausible range of axial vertical velocities ($3 \leq v_z \leq 18$ cm yr^{-1}) and plume excess temperature ($250 \leq \Delta T_p \leq 350$ °C), so that $450 \leq B \leq 3300$ kg s^{-1}. For each plume buoyancy flux we then test the stability field of a rheological heterogeneity ($1 < \lambda < 30$; $R_i = 40$ km). Fig. 6b shows that blob-like heterogeneities can be more easily preserved in plumes with a relatively low buoyancy flux, for example, if

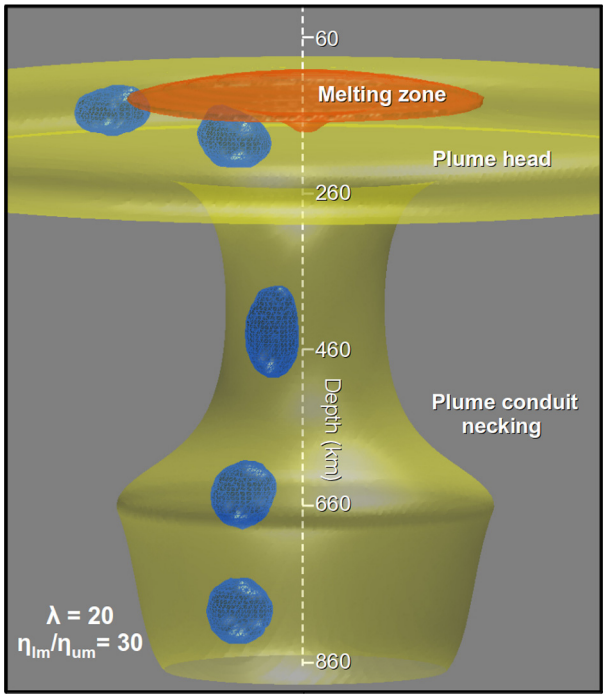

Fig. 7. The isosurface at excess potential temperature $\Delta T_p = 50$ °C (transparent yellow) shows plume conduit necking caused by the mantle viscosity contrast $\eta_{lm} = 30\eta_{um}$, modeled at 660 km depth. A viscous heterogeneity with $\lambda = 20$ and $R_i = 40$ km (shown in blue at different time steps) is able to maintain its blob-like shape.

$B = 1000$ kg s^{-1} the required λ is ~10, whereas if $B = 3000$ kg s^{-1} the viscosity ratio must be greater than 25. The buoyancy flux of several hotspots is reported in Fig. 6c, values by Sleep (1990), indicated with a star, often represent an upper bound with respect to the buoyancy flux range by King and Adam (2014). The Hawaiian hotspot is not included in the figure because its high buoyancy flux, 8700 kg s^{-1} for Sleep (1990) and up to 7100 kg s^{-1} for King and Adam (2014), is out of the range explored by our models.

Finally we consider the effect of a viscosity contrast between upper and lower mantle by modeling $\eta_{lm}/\eta_{um} = 30$ at 660 km depth. In the upper mantle the conduit radius is narrower, $r_{um} \sim 0.6 r_{lm}$ (Fig. 7), necking occurs because of plume flux conservation: a vertical velocity increase in the upper mantle must be accompanied by a reduction of the conduit radius. Both v_z and r variations act to enhance the strain rate and we find $\dot{\epsilon}_{um} \sim 3.3\dot{\epsilon}_{lm}$. It is thus legitimate to ask whether conduit necking can increase the deformation undergone by a viscous heterogeneities. Fig. 7 shows that a $\lambda = 20$ heterogeneity ($R_i = 40$ km) does maintain its blob-like shape, even when crossing the viscosity jump at 660 km depth and that the successive deformation, albeit visible, is relatively minor.

4. Discussion

Recycled eclogite (Hofmann and White, 1982), continent derived sediments (White and Hofmann, 1982; Jackson et al., 2007; Delavault et al., 2016) and recycled mantle lithosphere (Schaefer et al., 2002; Bizimis et al., 2007) are likely ingredients of mantle plumes. Although we know the geochemical fingerprints of these lithologies, their rheology remains elusive. Let us take the example of eclogite: at upper mantle P–T conditions, eclogite is a mineral assemblage of omphacite, the weakest of all pyroxenes, and of garnet, a strong mineral (Karato et al., 1995). The bulk viscosity of eclogite was found to be similar to that of harzburgite (Jin et al., 2001), but the viscosity contrast between eclogite

and peridotite remains poorly constrained. At lower mantle P–T conditions, eclogite is converted to an assemblage of bridgmanite, Ca-perovskite, Ca-ferrite and stishovite in similar proportions (Stixrude and Lithgow-Bertelloni, 2012). Ca-perovskite is characterized by a "shear softening" of the elastic response (Stixrude et al., 2007), however it is not straightforward to relate variations of the elastic constants to rheological properties, so that the bulk viscosity of a mafic composition in the lower mantle is also poorly constrained. In view of these uncertainties, we modeled rheological heterogeneities 5–30 times more viscous than the surrounding rocks, a range that does not seem to be ruled out by the current knowledge on rheological contrasts. We did not specify the causes of such a viscosity increase (e.g., composition, fluid content, grain size or geometry of the weak phase) and we took a fluid dynamics perspective, focusing on the flow perturbation caused by the rheological heterogeneity and on the deformation undergone by the heterogeneity.

We found that the blob-like shape is preserved at $\lambda = 4$ only for low strain rates ($\dot{\epsilon}_{xz} = 3\,10^{-15}$ s^{-1}), obtained at low values of the activation energy ($E = 140$ kJ mol^{-1}). For more plausible E and higher strain rate ($\dot{\epsilon}_{xz} = 3\,10^{-14}$ s^{-1}) a viscosity ratio $\lambda \geq 20$ is required to preserve the blob-like shape in a mantle plume. Moreover, the transition between high stretching (low λ) and negligible deformation ($\lambda \geq 20$) is not sharp and, at intermediate viscosity ratios ($\lambda \sim 10$), we discovered the existence of a transitional "tadpole" shape, with a blobby lower "head" and a narrow upper "tail".

We also explored to which extent the flow is perturbed by the presence of a rheological heterogeneity, with the question in mind whether this can cause intra-conduit mixing. The reduction of the vertical velocity inside a viscous blob perturbs the surrounding flow because the blob acts as an obstacle to the fluid column upwelling beneath it. This fluid tends to contour the blob, deviating toward the plume axis (upstream from the blob) and away from the plume axis (downstream from the blob). By looking at the deviation of the flow trajectories we estimated that the presence of a rheological heterogeneity perturbs the flow over a vertical distance of order $\sim 5R_i$ for R_i of 30–40 km. Nevertheless, our results do not bear out the predictions of Blichert-Toft and Albarède (2009) to the effect that rheological heterogeneities would cause cross-conduit mixing. In laminar flow we observe that the trajectories, after being locally displaced, recover their original position downstream from the heterogeneity. We do not find any significant radial mixing over a considerable spectrum of rheological contrasts. The persistent lateral heterogeneities within the plume, as documented by Abouchami et al. (2005) and confirmed by several subsequent studies (Huang et al., 2011; Weis et al., 2011), are consistent with this prediction.

We have shown that a rheological heterogeneity 20–30 times more viscous than the surrounding rocks does not mix, does not entrain, and does not deform significantly even while upwelling in a plume. This type of heterogeneity is thus ideally suited to preserve distinct isotopic signatures. In the following we argue that a rheological heterogeneity does carry a specific isotopic fingerprint, and we relate the time-scale of geochemical variability in hotspot lavas to the transit-time of the heterogeneity across the magma capture zone (MCZ) of a volcano. In contrast with a narrow filament, a 30–40 km radius blob can entirely fill the MCZ volume. This is important because the rheological heterogeneity will then produce 100% of the partial melt generated in the MCZ. The ensemble of these two conditions, (i) no long-time mixing of the rheological heterogeneity before melting and (ii) no mixing of melts once in the MCZ, is likely to cause a clear and distinct isotopic variation in lavas. Our results predict that such variations could last 0.5–1.0 Myr, the time-scale corresponding to the transit time of the blob (30–40 km radius) across the MCZ. For heterogeneities with a transitional shape, a precursory isotopic variation, lasting 1–1.5 Myr, will precede a more important variation of shorter duration (<0.5 Myr).

The geochemical variability induced by the mantle flow has a longer time-scale than the variability induced by processes taking place in the volcanic plumbing system. Therefore, in order to detect geochemical variations induced by the transit of rheological heterogeneities, it is necessary to study the isotopic evolution of hotspot lavas over time periods of several million years. For the Canary hotspot Taylor et al. (2017) analyzed Pb isotope variations over the last 10 Myr and found an interesting time variability: a given "Pb isotope trajectory" lasts for ∼1 Myr before changing, over a time-scale of ∼0.3 Myr, to another (parallel) trajectory lasting again ∼1 Myr. After ruling out a crustal origin, the authors interpret the observed trajectories as "pulses" of material emerging from the plume stem with a distinct $^{208}Pb^{\star}/^{206}Pb^{\star}$ ratio.[2] The $^{208}Pb^{\star}/^{206}Pb^{\star}$ reflects the ratio of $^{232}Th/^{238}U$ integrated over the Earth's history (Galer and O'Nions, 1985) and, because of the long half lives of ^{232}Th and ^{238}U, any measurable difference in $^{208}Pb^{\star}/^{206}Pb^{\star}$ cannot be created by recent changes in Th/U in the rock. We suggest that Taylor et al. (2017) "pulses" could correspond to blob-like rheological heterogeneities of radius 30–40 km, crossing the hotspot melting zone with time-scales of ∼1 Ma.

Interestingly, a weak buoyancy flux hotspot such as Canary, $B = 1000$ kg s^{-1} for Sleep (1990) and $B \leq 570$ kg s^{-1} for King and Adam (2014), is ideally suited to preserve blob-like rheological heterogeneities even at viscosity ratios $\lambda \leq 10$. For plumes with $1400 < B < 2000$ kg s^{-1} (e.g., Iceland, Samoa, Tristan, Réunion, using Sleep (1990) values) a blob will be stable for viscosity ratios ranging between 15 and 18, whereas for $B = 3300$ kg s^{-1} (e.g., Marquesas, Society, Pitcairn, using Sleep (1990) values) $\lambda \sim 30$ must be attained to preserve the blob-like shape. Given these results we can speculate that for the vigorous Hawaiian plume filaments and transitional-shapes will prevail even for $\lambda = 30$, and that blob preservation requires higher λ than what we considered here.

The different fate of rheological heterogeneities in weak *vs*. vigorous plumes could be a key aspect to interpret fundamentally different geochemical observations among Pacific hotspots. The French Polynesia hotspots forming the five main archipelagos (e.g., Society, Marquesas, Tuamotu, Gambier, Australs) are characterized by a large isotopic variability (Chauvel et al., 1992; Delavault et al., 2015) and by a discontinuous volcanic activity during the last 20 Myr. In contrast, Hawaiian lavas older than ∼4 Ma have a quite constant geochemical fingerprint, typical of the relatively depleted Kea-component (Tanaka et al., 2008; Harrison et al., 2017). The enriched Loa-component appeared only a few million years ago (Fekiacova et al., 2007; Tanaka et al., 2008) and the minor overlap in lead isotopes between Loa- and Kea-trend lavas clearly indicates that the two components are isotopically distinct (Abouchami et al., 2005). Yet, the total range of isotopic variability of Hawaiian lavas is much smaller than that observed for Polynesian hotspots lavas. According to Chauvel et al. (2012) this is due to different degrees of partial melting, because the low-degree melting at Polynesian hotspots preserves the source heterogeneities, whereas the high-degree melting of the Hawaiian hotspot blurs the isotopic variability. Here we suggest an additional possibility: in weak plumes blob-like heterogeneities are more easily preserved, and their geochemical fingerprint will clearly affect surface lavas, as discussed above. In vigorous plumes filament-like heterogeneities

[2] The radiogenic lead isotope ratio is defines as:

$$^{208}Pb^{\star}/^{206}Pb^{\star} = \frac{(^{208}Pb/^{204}Pb)_s - (^{208}Pb/^{204}Pb)_{pr}}{(^{206}Pb/^{204}Pb)_s - (^{206}Pb/^{204}Pb)_{pr}}, \quad (5)$$

where the subscript "s" stands for sample and "pr" for primordial.

should dominate, but, compared to blobs, their geochemical fingerprint might be more "blurred" simply because partial melts from a narrow filament represent, at any time, only a fraction of the melt produced in the MCZ.

Finally, if we speculate that a rheological heterogeneity might also be compositionally less fertile than the surrounding plume material, then its transit in the melting zone will cause a decrease in melt productivity. The effect will be particularly evident in low buoyancy flux hotspots, not only because blob-like heterogeneities are more likely to survive, but also because a decrease in melt productivity might lead to periods of discontinuous volcanism. French Polynesia hotspots have a discontinuous volcanic activity that is still unexplained. For Iceland the long-time (55 Ma) record of fluctuations in the volcanic activity has been attributed to temperature fluctuations of the plume (Parnell-Turner et al., 2014), possibly induced by the episodic generation of hot solitary waves. We suggest that the transit of rheological, less fertile, heterogeneities across the melting zone could represent an additional mechanism causing time variations of melt productivity on time-scales of order 1 Myr.

Our models have shown that finite size (30–40 km radius) rheological heterogeneities, 20–30 times more viscous than the surrounding rocks, remain unmixed and unstretched even in the high strain rate flow of a mantle plume. With these model results in mind, we have explored how rheological heterogeneities flowing across a hotspot melting zone might affect lava geochemistry and melt productivity. Future constraints from mineral physics should help to improve our understanding of what causes rheological differences in mantle rocks, and thus lead to a more specific interpretation relating rheology contrasts to time fluctuations of melt productivity and to plume geochemistry.

Acknowledgements

We thank Tim Jones and an anonymous reviewer for their thorough and constructive reviews. We also thank Catherine Chauvel for interesting discussions and John Brodholt for his editorial handling. Numerical computations were performed on the S-CAPAD platform, IPGP, France. C.G.F. was partly funded by PNP-INSU program. IPGP contribution No. 3958. LDEO Contribution No. 8234.

References

Abouchami, W., Hofmann, A.W., Galer, S.J.G., Frey, F., Eisele, J., Feigenson, M., 2005. Pb isotopes reveal bilateral asymmetry and vertical continuity in the Hawaiian plume. Nature 434, 311–326.

Ammann, M.W., Brodholt, J.P., Wookey, J., Dobson, D.P., 2010. First-principles constraints on diffusion in lower-mantle minerals and a weak D" layer. Nature 465, 462–465. https://doi.org/10.1038/nature09052.

Ballmer, M.D., Houser, C., Hernlund, J.W., Wentzcovitch, R.M., Hirose, K., 2017. Persistence of strong silica-enriched domains in the Earth's lower mantle. Nat. Geosci., 236–241. https://doi.org/10.1038/NGEO2898.

Becker, T.H., Kellogg, J.B., O'Connell, R.J., 1999. Thermal constraints on the survival of primitive blobs in the lower mantle. Earth Planet. Sci. Lett. 171, 351–365.

Bercovici, D., Ricard, Y., Richards, M.A., 2000. The relation between mantle dynamics and plate tectonics: a primer. In: Richards, M., et al. (Eds.), The History and Dynamics of Global Plate Motions. In: Geophysical Monograph, vol. 121. AGU, pp. 5–46.

Bizimis, M., Griselin, M., Lassiter, J.C., Salters, V.J.M., Sen, G., 2007. Ancient recycled mantle lithosphere in the Hawaiian plume: osmium–hafnium isotopic evidence from peridotite mantle xenoliths. Earth Planet. Sci. Lett. 257, 259–273.

Blichert-Toft, J., Albarède, F., 2009. Mixing of isotopic heterogeneities in the Mauna Kea plume conduit. Earth Planet. Sci. Lett. 282, 190–200.

Chauvel, C., Hofmann, A.W., Vidal, P., 1992. HIMU-EM: the French Polynesian connection. Earth Planet. Sci. Lett. 110, 99–119.

Chauvel, C., Maury, R.C., Blais, S., Lewin, E., Guillou, H., Guille, G., Rossi, P., Gutscher, M.A., 2012. The size of plume heterogeneities constrained by Marquesas isotopic stripes. Geochem. Geophys. Geosyst. 13, Q07005. https://doi.org/10.1029/2012GC004123.

Cordier, P., Amodeo, J., Carrez, P., 2012. Modelling the rheology of MgO under Earth's mantle pressure, temperature and strain rates. Nature 481, 177–180. https://doi.org/10.1038/nature10687.

Cox, R.G., 1969. The deformation of a drop in a general time-dependent fluid flow. J. Fluid Mech. 37, 601–623.

Delavault, H., Chauvel, C., Sobolev, A., Batanova, V., 2015. Combined petrological, geochemical and isotopic modeling of a plume source: example of Gambier Island, Pitcairn chain. Earth Planet. Sci. Lett. 426, 23–35.

Delavault, H., Chauvel, C., Thomassot, E., Devey, C.W., Dazas, B., 2016. Sulfur and lead isotopic evidence of relic Archean sediments in the Pitcairn mantle plume. Proc. Natl. Acad. Sci. 113, 12952–12956.

DePaolo, D.J., Stolper, E.M., 1996. Models of Hawaiian volcano growth and plume structure: implications of results from the Hawaii Scientific Drilling Project. J. Geophys. Res. 101, 11643–11654.

Farnetani, C.G., Hofmann, A.W., 2009. Dynamics and internal structure of a lower mantle plume conduit. Earth Planet. Sci. Lett. 282, 314–322. https://doi.org/10.1016/j.epsl.2009.03.035.

Farnetani, C.G., Hofmann, A.W., Class, C., 2012. How double volcanic chains sample geochemical anomalies from the lowermost mantle. Earth Planet. Sci. Lett. 359–360, 240–247.

Fekiacova, Z., Abouchami, W., Galer, S.J.G., Garcia, M.O., Hofmann, A.W., 2007. Origin and temporal evolution of Ko'olau volcano, Hawaii: inferences from isotope data on the Ko'olau Scientific Drilling Project (KSDP), the Honolulu volcanics and ODP Site 843. Earth Planet. Sci. Lett. 261, 65–83.

Ferrachat, S., Ricard, Y., 1998. Regular vs. chaotic mantle mixing. Earth Planet. Sci. Lett. 155, 75–86.

Galer, S.J.G., O'Nions, R.K., 1985. Residence time of thorium, uranium and lead in the mantle with implications for mantle convection. Nature 316, 778–782.

Harrison, L.N., Weis, D., Garcia, M.O., 2017. The link between Hawaiian mantle plume composition, magmatic flux, and deep mantle geodynamics. Earth Planet. Sci. Lett. 463, 298–309. https://doi.org/10.1016/j.epsl.2017.01.027.

Hirth, G., Kohlstedt, D.L., 1996. Water in the oceanic upper mantle: implications for rheology, melt extraction and the evolution of the lithosphere. Earth Planet. Sci. Lett. 144, 93–108.

Hofmann, A.W., White, W.M., 1982. Mantle plumes from ancient oceanic crust. Earth Planet. Sci. Lett. 57, 421–436.

Huang, S.C., Hall, P.S., Jackson, M.G., 2011. Geochemical zoning of volcanic chains associated with Pacific hotspots. Nat. Geosci. 4, 874–878. https://doi.org/10.1038/NGEO1263.

Jackson, M.G., Hart, S.R., Koppers, A.A.P., Staudigel, H., Konter, J., Blusztajn, J., Kurz, M., Russell, J.A., 2007. The return of subducted continental crust in Samoan lavas. Nature 448, 684–687. https://doi.org/10.1038/nature06048.

Jin, Z-M., Zhang, J., Green II, H.W., Jin, S., 2001. Eclogite rheology: implications for subducted lithosphere. Geology 29, 667–670.

Jones, T.D., Davies, D.R., Campbell, I.H., Wilson, C.R., Kramer, S.C., 2016. Do mantle plumes preserve the heterogeneous structure of their deep-mantle source? Earth Planet. Sci. Lett. 434, 10–17.

Karato, S., 2010. Rheology of the deep upper mantle and its implications for the preservation of the continental roots: a review. Tectonophysics 481, 82–98.

Karato, S., Wang, Z., Liu, B., Fujino, K., 1995. Plastic deformation of garnets: systematics and implications for the rheology of the mantle transition zone. Earth Planet. Sci. Lett. 130, 13–30. https://doi.org/10.1016/0012-821X(94)00255-W.

Katayama, I., Karato, S., 2008. Effects of water and iron content on the rheological contrast between garnet and olivine. Phys. Earth Planet. Inter. 166, 57–66.

Katz, R.F., Spiegelman, M., Langmuir, C.H., 2003. A new parametrization of hydrous mantle melting. Geochem. Geophys. Geosyst. 4. https://doi.org/10.1029/2002GC000433.

King, S.D., Adam, C., 2014. Hotspot swells revisited. Phys. Earth Planet. Inter. 235, 66–83.

Manga, M., 1996. Mixing of heterogeneitieis in the mantle: effect of viscosity differences. Geophys. Res. Lett. 23, 403–406.

Merveilleux du Vignaux, N., Fleitout, L., 2001. Stretching and mixing of viscous blobs in Earth's mantle. J. Geophys. Res. 106, 30893–30908.

O'Connell, R.J., Gable, C.W., Hager, B.H., 1991. Toroidal–poloidal partitioning of lithospheric plate motion. In: Sabadini, R., et al. (Eds.), Glacial Isostasy, Sea Level and Mantle Rheology. Kluwer Academic, Norwell, Mass., pp. 535–551.

Olson, P., Schubert, G., Anderson, C., 1993. Structure of axisymmetric mantle plumes. J. Geophys. Res. 98, 6829–6844.

Parnell-Turner, R., White, N., Henstock, T., Murton, B., Maclennan, J., Jones, S.M., 2014. A continuous 55-million-record of transient mantle plume activity beneath Iceland. Nat. Geosci. 7, 914–919. https://doi.org/10.1038/NGEO2281.

Schaefer, B.F., Turner, S., Parkinson, I., Rogers, N., Hawkesworth, C., 2002. Evidence for recycled Archean oceanic mantle lithosphere in the Azores plume. Nature 420, 304–307.

Sleep, N.H., 1990. Hotspot and mantle plumes: some phenomenology. J. Geophys. Res. 95, 6715–6736.

Spence, D.A., Ockendon, J.R., Wilmott, P., Turcotte, D.L., Kellogg, L., 1988. Convective mixing in the mantle: the role of viscosity differences. Geophys. J. 95, 79–86.

Stixrude, L., Lithgow-Bertelloni, C., Kiefer, B., Fumagalli, P., 2007. Phase stability and shear softening in $CaSiO_3$ perovskite at high pressure. Phys. Rev. B 75, 024108. https://doi.org/10.1103/PhysRevB.75.024108.

Stixrude, L., Lithgow-Bertelloni, C., 2012. Geophysics and chemical heterogeneitiy in the mantle. Annu. Rev. Earth Planet. Sci. 40, 569–595.
Tackley, P.J., 1998. Three-dimensional simulations of mantle convection with a thermo-chemical basal boundary layer: D"? In: Gurnis, M. (Ed.), The Core–Mantle Boundary Region. In: Geophys. Monogr., vol. 28. AGU, Washington, D.C., pp. 231–253.
Takeda, Y., 1998. Flow in rocks modelled as multiphase continua: application to polymineralic rocks. J. Struct. Geol. 20, 1569–1578.
Tanaka, R., Makishima, A., Nakamura, E., 2008. Hawaiian double volcanic chain triggered by an episodic involvement of recycled material: constraints from temporal Sr–Nd–Hf–Pb isotopic trend of the Loa-type volcanoes mantle with implications for mantle convection. Earth Planet. Sci. Lett. 265, 450–465.
Taylor, G.I., 1934. The formation of emulsions in definible fields of flow. Proc. R. Soc. Lond. Ser. A, Math. Phys. Sci. 146, 501–523.
Taylor, R.N., Farley, E.R., Davilaharris, P., Branney, M., Gernon, T.M., 2017. Pulsing evolution of a hotspot: constraining the scale of mantle heterogeneities. Goldschmidt 2017 Abstract.
Turcotte, D.L., Schubert, G., 1982. Geodynamics. Applications of Continuum Physics to Geological Problems. J. Wiley, New York, p. 450.
van Keken, P.E., Davaille, A., Vatteville, J., 2013. Dynamics of a laminar plume in a cavity: the influence of boundaries on the steady state stem structure. Geochem. Geophys. Geosyst. 14, 158–178. https://doi.org/10.1029/2012GC004383.
Weertman, J., 1970. The creep strength of the Earth's mantle. Rev. Geophys. Space Phys. 8, 145–168.
Weis, D., Garcia, M.O., Rhodes, J.M., Jellinek, M., Scoates, J.S., 2011. Role of the deep mantle in generating the compositional asymmetry compositional asymmetry of the Hawaiian mantle plume. Nat. Geosci. 4, 831–838. https://doi.org/10.1038/NGEO1328.
White, W.M., Hofmann, A.W., 1982. Sr and Nd isotope geochemistry of oceanic basalts and mantle evolution. Nature 296, 821–825.
Yamazaki, D., Karato, S., 2001. Some mineral physics constraints on the rheology and geothermal structure of Earth's lower mantle. Am. Mineral. 86, 385–391.
Yamazaki, D., Kato, T., Yurimoto, H., Ohtani, E., Toriumi, M., 2000. Silicon self-diffusion in $MgSiO_3$ perovskite at 25 GPa. Phys. Earth Planet. Inter. 119, 299–309.
Zerr, A., Boehler, R., 1994. Constraints on the melting temperature of the lower mantle from high-pressure experiments on MgO and magnesiowustite. Nature 371, 506–508. https://doi.org/10.1038/371506a0.